RESEARCH ARTICLE

Flexible photocatalytic membrane based on CdS/PMMA polymeric nanocomposite films: multifunctional materials

Mai S. A. Hussien [1,2] · Mervat I. Mohammed [2] · Ibrahim S. Yahia [3,4,5]

Abstract

In this study, poly(methyl methacrylate) with different doping nano-cadmium sulfide (CdS/PMMA) is prepared and characterized. CdS/PMMA polymeric nanocomposite films were synthesized using solution casting methodology. SEM and XRD are used for structure analysis for the studied nanocomposite films. XRD revealed the amorphous domains of PMMA polymer, which increased with increasing CdS nanoparticle contents. SEM revealed the CdS dispersion within the PMMA matrix. CdS nanoparticles in the PMMA matrix are expected to be aggregated due to the casting technique. The optical energy gap is found to be decreased after the CdS addition. ε' and ε'' have the same behavior with the applied frequency. Maxwell-Wagner interfacial polarization is the responsible factor for higher values of $\varepsilon'–\varepsilon''$ at the higher frequencies. Electrical conductivity behavior σ_{AC} tends to obtain a constant value at lower frequencies that approach from its DC conductivity values. After doping PMMA with nano-CdS, an exponential increase after a critical frequency value and the values of σ_{AC} was also increased. Besides, a significant reduction in laser energy power is identified by the reduction of the output power. CdS/PMMA can attenuate the laser power due to its nonlinear effect. CdS/PMMA nanocomposite can act as a photocatalyst to improve the performance of the photodegradation of Rhodamine B (RhB). Among the different CdS/PMMA nanocomposite films, 3.33 wt% CdS/PMMA demonstrates the highest efficiency in visible photocatalysis of Rhodamine B. CdS/PMMA can be utilized as multifunctional materials use like laser optical limiting to reduce the power of laser sources and as a photocatalyst membranes.

✉ Mai S. A. Hussien
maisalehamar@gmail.com; maisaleh@edu.asu.edu.eg

[1] Department of Chemistry, Faculty of Education, Ain Shams University, Roxy, Cairo 11757, Egypt

[2] Nanoscience Laboratory for Environmental and Biomedical Applications (NLEBA), Metallurgical Lab.1., Department of Physics, Faculty of Education, Ain Shams University, Roxy, Cairo 11757, Egypt

[3] Research Center for Advanced Materials Science (RCAMS), King Khalid University, P.O. Box 9004, Abha 61413, Saudi Arabia

[4] Advanced Functional Materials & Optoelectronic Laboratory (AFMOL), Department of Physics, Faculty of Science, King Khalid University, P.O. Box 9004, Abha, Saudi Arabia

[5] Semiconductor Lab., Department of Physics, Faculty of Education, Ain Shams University, Roxy, Cairo 11757, Egypt

Introduction

Attention has been attracted to the homogeneous polymeric matrix with organic/inorganic contents. These new composites exhibit highly interesting and versatile applications. Metal sulfides/polymer nanocomposites are promising materials with particular characteristics. They can be applied in numerous fields, like light-emitting diodes, solar cells, chemical change, optoelectronic devices, photodetectors, and sensors (Mthethwa et al. 2011; Ranjbar et al. 2013). Recently, polymers incorporated with semiconductor particles form new composites with new physical characteristics like electrical and optical features, which can be used in photocatalytic and photoelectrical applications (Chan et al. 2017).

Cadmium sulfide has $E_g = 2.42$ eV with promising features in optoelectronics. The adjustable bandgap leads to some uses such as quantum computing, data storage, photovoltaic cells, and optical devices (Venkatram et al. 2005; Miao et al. 2009). Jie Jiao et al. found that PbS and CdS quantum dots are highly performed

in applications of solar cells (Jie et al. 2013). Characteristics and performance of nano-CdS were affected by their size.

PMMA has unique mechanical and chemical-physical properties (Ajibade and Mbese 2014; Dixit et al. 2009). The polymer's selection depends on its magnetic, mechanical, optical, and thermal characteristics. Other properties, such as chemical stability and functionalities, hydrophilic/hydrophobic, and biocompatibility properties, were considered during the composite formation (Jeon and Baek 2010). It has -COOCH$_3$ group, 1.6 Debye dipole moment, and 3.4 dielectrics (Chan et al. 2017). It can be utilized in many technological and productive areas (Kondawar et al. 2011; Zhang et al. 2011). Some disadvantages have reduced global use to PMMA, such as the insufficiency of UV-light filters and thermal sensitivity. Still, the incorporation of some semiconductors may overcome some of these drawbacks (Zhao et al. 2008; Ummartyotin et al. 2012).

The development of effective, low-cost water treatment techniques is essential to human health (Mai and Yahia 2019). Heterogeneous photocatalysis is a popular way using semiconductor catalysts such as ZnS, ZnO, Fe$_2$O$_3$, TiO$_2$, PbS, and CdS (Pichat 2013). The polymeric nanocomposites have a combination of characteristics of nanomaterials with polymer properties, such as high durability, flexible nature, chemical resistance, low density, mechanical stability, ease of availability, and low cost (Hafizah et al. 2013). PMMA is considered a widespread suitable material with thermoplastic features to water contact (Motaung et al. 2012).

Photocatalytic oxidation technology is a practical, low-cost strategy for the degradation of the contaminants in wastewater; it takes less time than traditional technologies (Murcia López et al. 2017). In the photocatalytic process, semiconductors obtain chemical energy from the transformation of absorbed light energy (Tsai et al. 2017). There have recently been comprehensive efforts to inhibit photo-corrosion and improve CdS performance. It was announced by Wang et al. (2017) that covering CdS with impermeable graphene layers leads to improving the resistivity. Ai et al. (2018) solved the photo-corrosion of CdS through the intersection of the appropriate phase between both hexagonal and cubic phases of CdS according to the band engineering theory. These materials maintained high stability and optimum photocatalytic activity higher than single-phase materials. Furthermore, Ning et al. (2018) got water-splitting photostable CdS nanoparticles by insertion Al$_2$O$_3$. On the premise of the above strategies, it has been proved that CdS is an excellent photocatalyst due to its activity and stability.

Sol-gel, in situ polymerization, and blending are examples of methods that can be used to obtain semiconductor/polymer photocatalyst membranes. In situ polymerization is a simple process with a simple reaction condition, so it was prevalently used. Wang et al. (2008) improved TiO$_2$ with PPy through the in situ way, in which PPy/TiO$_2$ composites exhibited greater photoactivity than neat TiO$_2$ nanoparticles for the degradation of methyl orange under sunlight illumination.

Herein, the effect of CdS nano-fillers in the PMMA matrix was studied. In this study, some necessary analysis was done, such as X-ray diffraction (XRD) and scanning electron microscopy (SEM) for the structure confirmation. In the later part, the effects of frequency, CdS concentrations, and laser power on the PMMA/CdS polymeric nanocomposites were examined by measuring the absorbance, transmittance, optical bandgap, absorption index, dielectric properties, and AC electrical conductivity. The studied nanocomposite films showed a higher control of the laser power CUT-OFF laser filter, i.e., laser power attenuation. CdS/PMMA showed a significantly superior visible photocatalytic activity related to the pure PMMA. This may be due to the significant synergistic effect among CdS and PMMA. Moreover, the visible photocatalytic mechanism for CdS/PMMA membranes was proposed and analyzed.

Experimental details

Preparation of CdS nanoparticles

The co-precipitation method was applied to synthesis CdS nanoparticles. First, 0.5 M of cadmium nitrates and 0.5 M sodium sulfide (Na$_2$S) were dissolved in aqueous media for 1 h using hotplate/magnetic stirrer operated at (60 °C and 700 rpm). After that 100 ml of cetyltrimethylammonium bromide (CTAB) of 10 g/l was used as a surfactant. Na$_2$S was poured dropwise to form a yellow precipitate. The reaction was left at 60 °C for another 1 h to complete the reaction. The yellow precipitate was washed several times by distilled water to remove any residuals or sodium ions from the solution. After that, the CdS precipitate was applied for drying at 100 °C for 24 h.

Preparation of CdS/PMMA polymeric nanocomposites films

The solution casting process was applied to get CdS/PMMA polymeric nanocomposite films. We dissolve 20 g PMMA powder in 200 ml chloroform (high grade) using magnetic stirring for 48 h/700 rpm at room temperature. Different weight percent of CdS (0, 0.033, 0.166, 0.33, 3.33 wt%) were uniformly dispersed in PMMA solution using ultrasonic homogenizer for 5 min at 100 W. Flat-bottomed Petri dish was used for the casting solutions of pure and CdS/PMMA solutions until the complete drying at room temperature and was saved in the dark area. All CdS/PMMA films were removed from the Petri dish after 5 days.

Measurement techniques

Shimadzu LabX-XRD-6000 with CuK_α ($\lambda = 1.5406$ Å) was utilized to get the XRD patterns of CdS/PMMA films.

The JSM-6360 scanning electron microscope operated at 20 kV (SEM) was hired to reach the morphological structure of studied samples.

Linear optical characteristics were obtained by the JASCO V-570 spectrometer in the wavelength region 230 nm to 2500 nm operated at room temperature.

Dielectric properties were determined using an LCR meter (model FLUKE-PM-6306) at room temperature. Two probe designed holder was made from Teflon, and brass was used for AC conductivity and dielectric properties without using silver paste. The upper electrode was made from brass with a gentle spring to have excellent contact with the upper sample contact.

The Z-scan system, including the optical rack, holder, lens, and detector, was utilized for the estimation of the optical limiting. The samples were fixed and inserted on the focal point of the lens with focal length = 10 cm. The optical laser power meter was inserted after the sample holder. A laser source beam was obtained from the red He-Ne laser operated at 632.8 nm, and a green laser diode was operating at 532 nm. Newport, photodetector model-1916R, was hired to get output/input power of the laser with/without samples, respectively. A suitable fixed holder was designed and used.

Photocatalytic activity studies

A 200 ml of RhB (i.e. its concentration 10 mg/L) through a visible-wooden photoreactor was used to evaluate the sample photocatalytic activity. The photoreactor was designed by I.S. Yahia and his group in NLEBA, Ain Shams University (ASU), Egypt, as shown in Fig. 1. The reactor has two parts named as external and internal sections. It consists of a wooden design in the outside part with a height of 100 cm, a length of 95 cm, and a width of 65 cm. Inside, there are seven white lamps of wavelength (400–700 nm) nm of 18-W power and seven blue light lamps of 18-W power, each with a spectrum more significant than 420 nm. Each lamp is controlled individually. ON/OFF push-buttons were used to control the system. To keep the temperature constant inside the photoreactor at room temperature, a high-quality air fan was attached to the system to circulate the air within the system. During the experiments, the sample was stirred using a 15 multi-position magnetic stirrer. During the time of light irradiation, the distance between the lamps and the sample was fixed.

CdS/PMMA membranes were added to RhB about 200 ml aqueous mixture at ambient temperature. The mixture was stirred about 60 min using a magnetic stirrer without any illumination to obtain CdS/PMMA of different concentrations/ RhB adsorption-desorption equilibrium. A total of 5 ml of the suspension was drawn every 5 min interval from the mixture through the irradiation process.

JASCO V-550, Japan UV-Vis double beam spectrophotometer, was applied for determining the remaining RhB concentration through the absorbance data/plots. This scan was repeated for 5 cycles to check the reusability and stability of the synthesized samples.

Results and discussion

XRD patterns of CdS/PMMA nanocomposite membranes

X-ray diffraction patterns of pure CdS, pure PMMA, and the other prepared CdS/PMMA polymeric nanocomposites are shown in Fig. 2. XRD pattern for nano-CdS nanoparticles reveals the characteristic peaks of the hexagonal wurtzite structure for the crystalline CdS. The XRD pattern of a typical CdS nanoparticles exhibits prominent broad peaks at 2θ

Fig. 1 Photoreactor design and operation in NLEBA, Ain Shams University, Cairo, Egypt
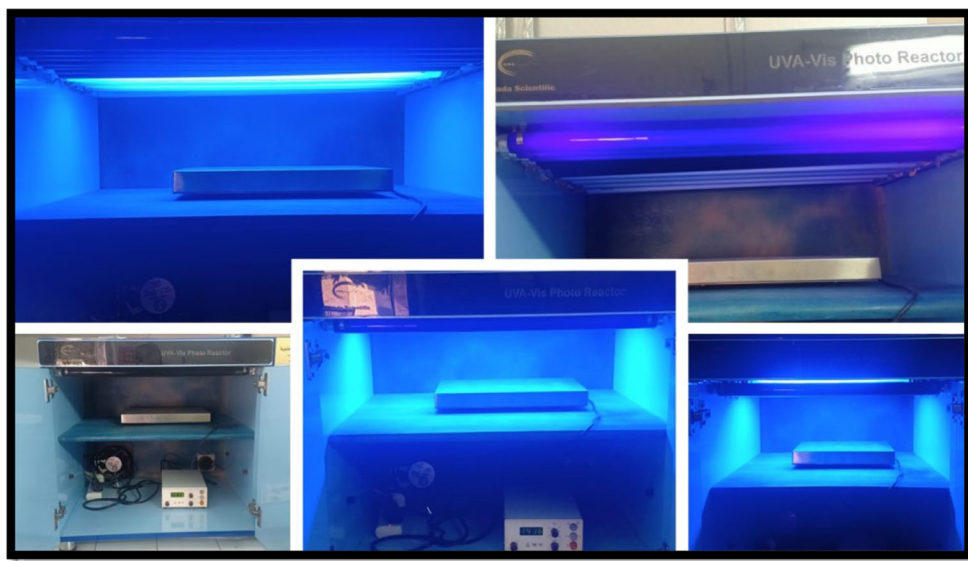
values of 26.54°, 43.52°, and 51.49° which could be indicated as scattering from the (111), (220), and (311) cubic phase CdS plans, respectively (Al-Hussam and Jassim 2012). The diffraction peaks in XRD patterns of nano-CdS have been indexed to be consistent with the standard values for CdS given in the JCPDS file (80-006). XRD patterns have diffraction peaks at 31.30°, 34.15°, 35.83°, 47.24°, and 56.30° for CdS. In contrast, the pure PMMA has 16.11° and 31.95° broad peaks, which are compatible with JCPDS-79-0208 (Mohammed and Yahia 2018; Mohammed 2018), indicating the polymeric amorphous behavior of pure PMMA. CdS/PMMA showed a loading impact. The broadness of the amorphous hump of CdS/PMMA was affected by CdS loading contents. Upon raising the CdS concentrations in PMMA matrix, the peaks 26.54°, 43.52°, and 51.49° were broaden and compatible with the diffraction planes of cubic CdS named [111], [220], and [311], respectively (Mohamed et al. 2014) (JCPDS file No. [00-10-454]) (Tripathi et al. 2015).

Morphological characterization

SEM was used to create a high-resolution nanocomposite images to monitor the particle size of samples. SEM images of pure PMMA are evidenced through Fig. 3a. Pure PMMA surface indicates that PMMA is smoothed. SEM images of different loading of CdS/PMMA nanocomposites films were obtained in Fig. 3b–f. The dispersion of as-prepared CdS/PMMA has been evaluated via increasing its density by increasing the CdS loading through PMMA. Increasing the CdS content leads to agglomeration, and size increase in CdS/PMMA. The smoothed surface area was diminished by raising the concentration of CdS. Vishal and Sharma (2013)
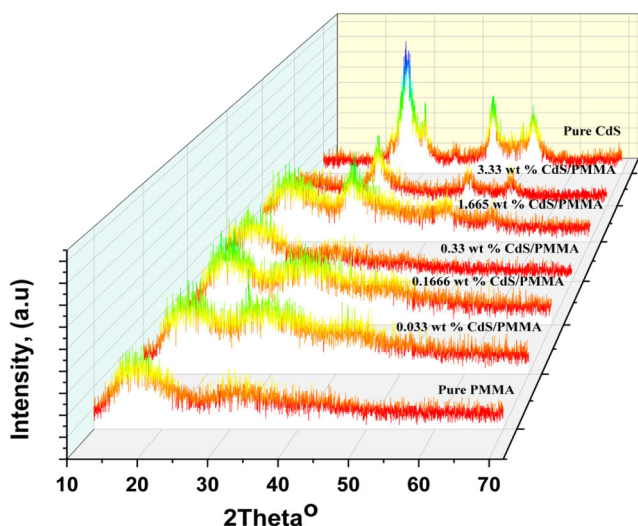

Fig. 2 X-ray diffraction patterns of CdS, PMMA, and CdS/PMMA nanocomposite films with different content of CdS nanoparticles

informed that the CdS/PMMA matrix is created by exfoliation of CdS through the polymeric void sites.

Optical analysis studies of CdS/PMMA nanocomposite films

For the CdS/PMMA nanocomposite film, the transmittance as a function of wavelength was elucidated in Fig. 4a, b. The pure PMMA has ~ 80% transparency with a decrease in its values by increasing CdS contents, and the $T(\lambda)$ values equal to zero for 3.33 wt%, as seen from Fig. 4a. $T(\lambda)$ is increased by increasing the wavelength up to 1600 nm after that the interaction of light with polymer/dopants materials. Figure 4b represents the transmittance of the studied samples in the wavelength region from 230 to 800 nm for more illustrations. The light transparency of CdS/PMMA nanocomposite films is decreased due to the CdS loadings in the PMMA matrix.
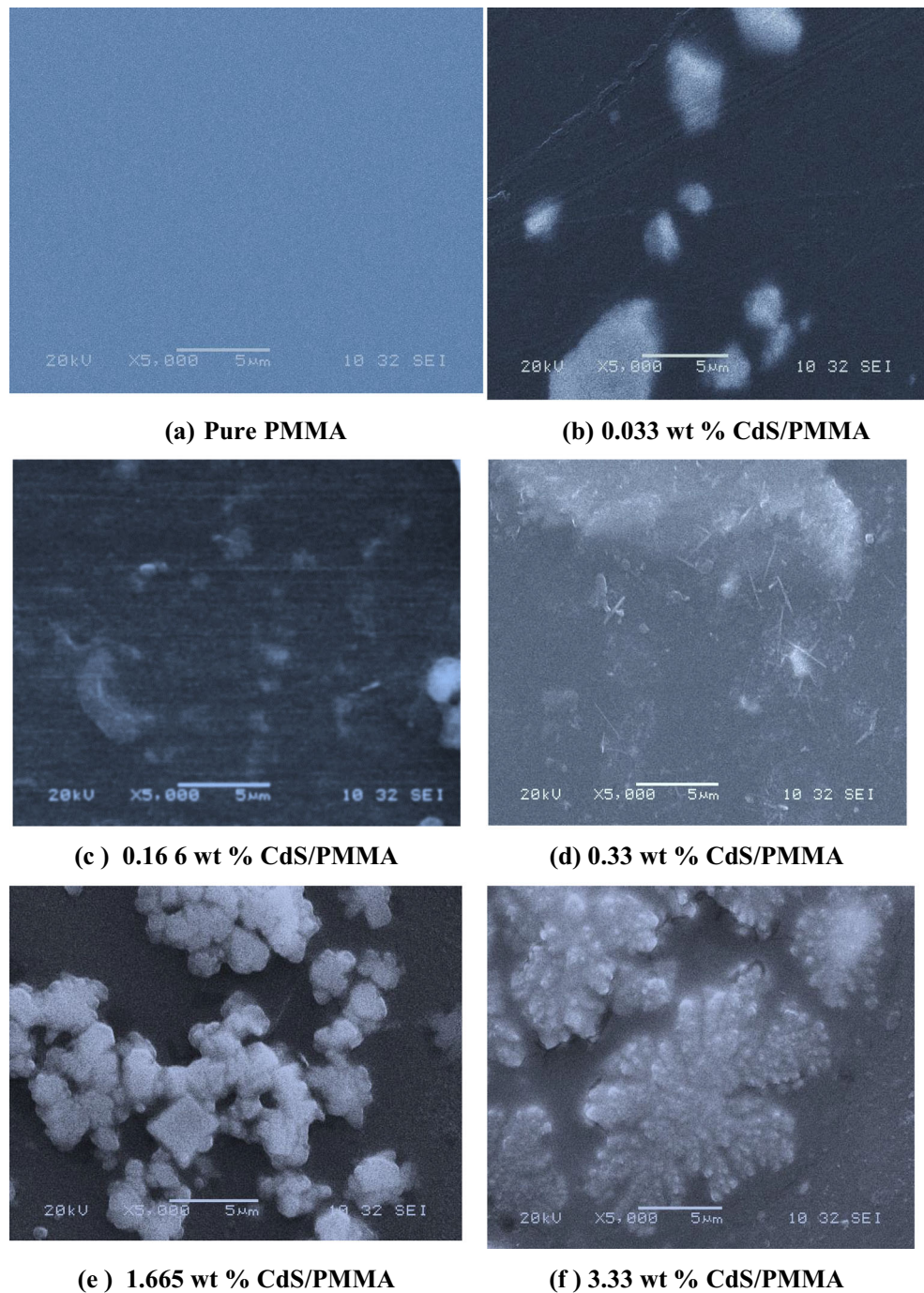
Figure 5 shows the absorption spectrum of CdS/PMMA nanocomposite films. Absorption spectra of the studied samples showed a decrease in its values with wavelength while it is increased with increasing the CdS contents. Cadmium sulfide has free electrons to enhance the electromagnetic performance, which is compatible with the previously reported work (Mervat et al. 2018). UV-Vis absorption bands of CdS/PMMA are inspected on antibonding–bonding, π-π* transitions (Choudhary and Sengwa 2016; Choudhary 2017; Mansour Sh et al. 2016). The following equation was used to calculate the optical bandgap (E_g) (Dang et al. 2004). The absorption value of pure PMMA is less absorbed than the other nanocomposites and rises with the increase of CdS nanoparticles (Heiba et al. 2017). For all CdS/PMMA nanocomposites, the absorption shoulder peak is detected between 320 and 570 nm. CdS nanoparticles in the nanocomposites showed the appearance of the absorption shoulder. This absorption shoulder is ascribed to a bound exciton in crystalline nanoparticles. This may be attributed to the following parameters: particles, shape, surface structure, defect concentration, and charge (Padmaja et al. 2013).

Tauc's plots were drawn to get an optical energy gap. Devis and Mott's equation was used to obtain the absorption coefficient as a function of the light photon energy as (Tauc et al. 1970):

$$(\alpha h\upsilon)^2 = B^2 \left(h\upsilon - E_g^d\right) \tag{1}$$

where the Planck's constant is h, the constant is B, the energy bandgap is E_g among the conduction and valence bands, and the absorption coefficient is α represented the symbol description of Eq. 1. The absorption coefficient can be determined by the following equations: $\alpha = 2.303A/d$ where the absorbance (Abs) and the film thickness d are the main components of this equation. Figure 6a and b represent the plots between $(\alpha h\upsilon)^2$ and $(\alpha h\upsilon)^{1/2}$ versus $h\upsilon$ to get direct and indirect bandgaps for

Fig. 3 SEM micrographs of **a** pure PMMA and CdS/PMMA nanocomposite films with **b** 0.033 wt%, **c** 0.166 wt%, **d** 0.33 wt%, **e** 1.665 wt%, and **f** 3.3 wt% of CdS

(a) Pure PMMA

(b) 0.033 wt % CdS/PMMA

(c) 0.16 6 wt % CdS/PMMA

(d) 0.33 wt % CdS/PMMA

(e) 1.665 wt % CdS/PMMA

(f) 3.33 wt % CdS/PMMA

possible transition through the extrapolation the straight lines to $h\upsilon$ = zero (Ismail et al. 2012). The obtained values of the bandgap for direct and indirect transitions are mentioned in Table 1. It is observable that CdS insertion in the PMMA matrix diminishes the E_g due to the defects generated in the studied nanocomposite films, causing a reduction of the bandgap. The reasons for these defects lie in the localized states in the bandgap, which reproduce the disorder degree in extended samples, which can be the leading cause of the generation charge transfer complexes (CTC) between HOMO and LUMO energy bands that make lower energy transfers possible due to interaction/coordinated PMMA chains and CdS NPs. Also, this decrease in the bandgap may be attributed to the presence of unstructured defects, which increase the density of localized states in the bandgap. The decrease in the optical gap with increasing the doping level results in a decrease in the degree of crystallinity of the represented films. These results are confirmed from the XRD analysis of the investigated film samples. These values are in good agreement with the values obtained previously. This performs previously
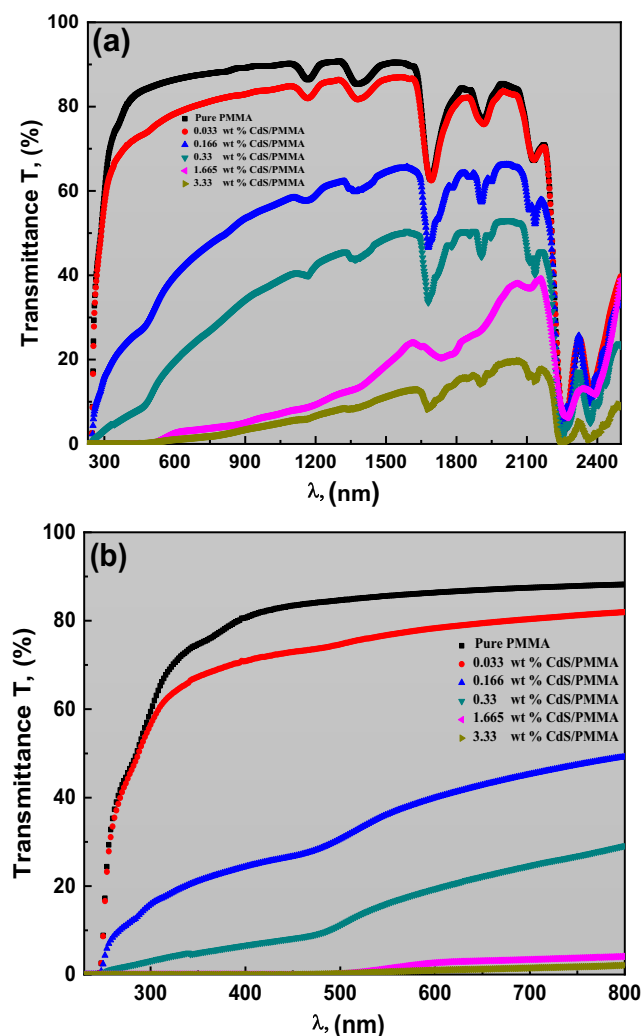
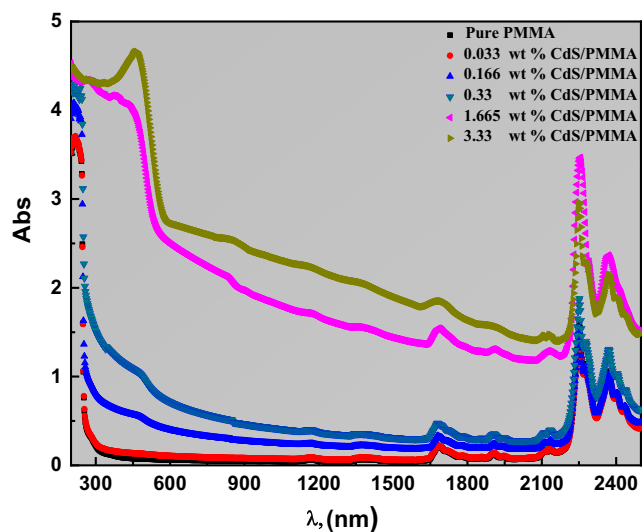**Fig. 4** Transmittance spectra of CdS/PMMA nanocomposites films **a** from 230 to 2500 nm, and **b** from 230 to 800 nm

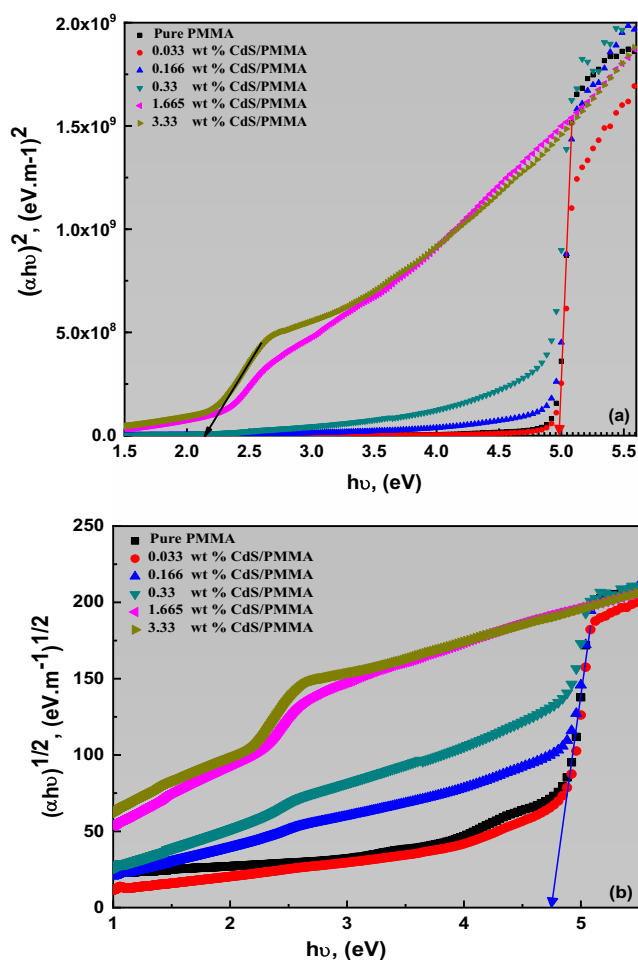**Fig. 5** Absorbance spectra versus wavelengths of CdS/PMMA nanocomposite films

Fig. 6 The plot of **a** $(\alpha h\upsilon)^2$, **b** $(\alpha h\upsilon)^{1/2}$ vs. photon energy $(h\upsilon)$ of CdS/ PMMA nanocomposite films

described when studied the CdS/PMMA by Vishal et al. (2013) and Padmaja et al. (2015), CdS/PEO by Padmaja et al. (2013), CdS/PVA by Al-Taay et al. (2016), and CdS/ PS by Vishal et al. (2013) (see Table 1). The bandgaps enhanced the light absorption behavior for the polymer nanocomposites.

Figure 7 illustrates the variation of the extinction coefficient of CdS/PMMA films with the wavelength. The behavior of k was increased by increasing the wavelength and the CdS contents. The absorption has been raised at the edge of the absorption region because of electronic transitions lead to the increase of the absorption coefficient.

Dielectric properties and AC electrical conductivity of CdS/PMMA nanocomposite films

Dielectric constants of CdS/PMMA nanocomposite films

The dielectric constant $(\varepsilon^{'})$ as a real complex dielectric constant part of CdS/PMMA nanocomposite films was

Table 1 The optical bandgap (indirect and direct) of PMMA/CdS nanocomposite films in comparison with recent studies

Bandgap/polymer nanocomposite	E_g^{ind}, (eV)	E_g^d, (eV)	
Pure PMMA	4.69	4.90	Present work
0.033 wt% CdS/PMMA	4.72	4.86	
0.16 wt% CdS/PMMA	4.487	4.85	
0.33 wt% CdS/PMMA	4.39	4.78	
1.665 wt% CdS/PMMA	1.5	2.18	
3.33 wt% CdS/PMMA	1.33	2.15	
PMMA/CdS	---	2.94–3.01	Vishal et al. (2013)
PMMA/CdS	---	3.09	Padmaja et al. (2015)
PS/CdS	---	3.44	Vishal et al. (2013)
PVA/CdS	----	2.55 2.4	Al-Taay et al. (2016)
CdS/PEO	----	2.54–2.45	Padmaja et al. (2013)
PMMA/CdS	----	3.25–2.54	Padmaja et al. (2014)

calculated at 30 °C from the relation (Mervat et al. 2018):

$$\varepsilon' = \frac{Cd}{\varepsilon_o A}, \qquad (2)$$

where the measured capacitance is C, the thickness is d, and the cross-section area is A. The dielectric loss (ε'') as an imaginary complex dielectric constant part was obtained through the equation (Mervat et al. 2018):

$$\varepsilon'' = \varepsilon' \tan\delta \qquad (3)$$

where the loss tangent is $\tan\delta$ which represents the loss during the applied AC field. Both the dielectric loss and dielectric constant are illustrated in Fig. 8a and b, which are functions of the applied frequency for CdS/PMMA films. The capacitance depends on the dielectric

Fig. 7 Extinction index as a function of the wavelength of CdS/PMMA nanocomposite films

constant because it is proportional to polymeric specimen surface charge storage through the subjected to the electric field (Parthibavarman et al. 2014). At the frequency region from 10 to 1 MHz, CdS/PMMA dielectric became frequency independent while dielectric loss and dielectric constant rise per decrease the applied frequency, which revealed the non-Debye manner at the lower frequency. This caused by the generation of free charge at the lower frequencies due to the interfacial polarization. The interfacial polarization was responsible for increasing both ε' and ε'' values according to Maxwell-Wagner-Sillars (MWS) (Sugumaran et al. 2015) which results from piling up the charges on the interfaces of various components in the nanocomposite leading to the construction of micro-capacitances over the whole material. This contributes to the increasing ε' and ε'' at the lower frequencies. The dipole was changed because of the interactions between polar functional groups in PMMA structure and CdS nanoparticles. This attitude causes the rise of ε' and ε'' with increasing CdS content (Choudhary 2017).

AC electrical conductivity analysis of CdS/PMMA nanocomposites films

AC electrical conductivity of CdS/PMMA was evaluated by Kashiwagi et al. (2007), Mervat et al. (2018), and Maji et al. (2015):

$$\sigma_{Total.AC}(\omega) = \frac{t}{ZA}, \qquad (4)$$

$$\sigma_{Total.AC}(\omega) = \sigma_{DC}(\omega \to 0) + \sigma_{AC}(\omega), \qquad (5)$$
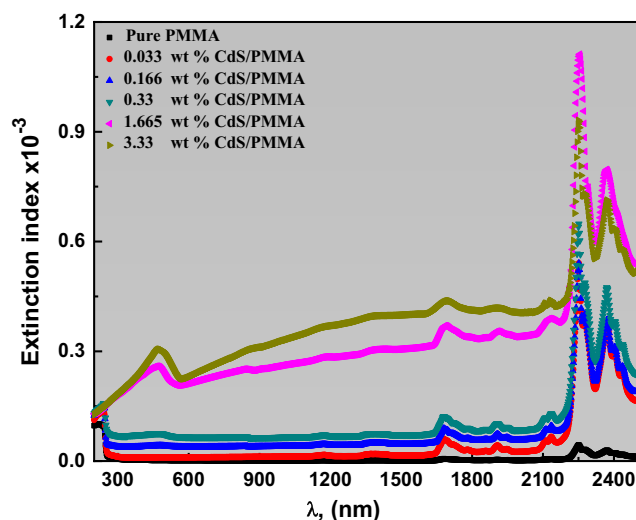
$$\sigma_{AC}(\omega) = A\omega^s, \qquad (6)$$

Fig. 9 The variation of AC electrical conductivity with $ln\omega$ of CdS/ PMMA nanocomposite films

Fig. 8 Schematic curves for frequency dependent of **a** ε' and **b** ε'' of CdS/ PMMA nanocomposite films

The total AC electrical conductivity is $\sigma_{Total.AC}(\omega)$, the measured impedance is Z, and A is a constant depending on the temperature, $\sigma_{DC}(\omega \rightarrow 0)$ and $\sigma_{AC}(\omega)$ are the DC and AC electrical conductivities, the angular frequency is $\omega = 2\pi f$, and the frequency exponent is denoted as (s). Figure 9 showed the AC electrical conductivity (σ_{AC}) varied with frequencies. σ_{AC} is not affected by varying the frequency at the lower frequencies, until a critical frequency, and the behavior is versed. Disordered solids obey this manner according to AC universal law revealing the hopping mechanism for the charge migration. Many electrons are subjected to a composite conducting band by increasing the CdS content. The rising frequency improves the hopping frequency polarity leading to a plateau in both low and high-frequency regions. Available free charges let the electrical conductivity by a frequency independent at lower frequency region while trapped charges and so, a dependent at the higher frequency region is expected (Maji et al. 2015). The electrical conductivity of CdS/PMMA films has higher than the pure PMMA due to facile electron-hole hopping in the conduction process (Al-Hosiny et al. 2013).
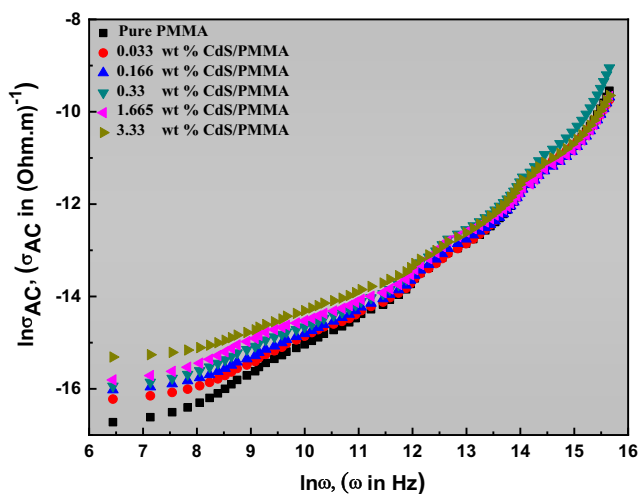
The optical limiting of CdS/PMMA nanocomposites films

Facile costless optical limiting flexible nanocomposite films were urgently progressed to fabricate optical and eye-protective laser sensors. Laser radiation power density was diminished by optical limiters to safeguard laser sensitive and delicate eye. CdS/PMMA is studied for its applications in optical limiting filters using two different laser beams (i.e., the green laser diode operated at 532 nm and the red He-Ne laser operated at 632.2 nm) using the same conventional Z-scan experimental technique (here, the samples remain constant).

Figure 10 reveals the normalized power curves versus wt% of CdS content. The normalized power equals the input/output power. PMMA slightly restricted energy intensity impact as normalized yield energy. The concentration of the nano-CdS fillers plays an essential role in the restrictive optical impact. The increases of CdS content in PMMA are contributed to the absorption processes interaction, i.e., increased the sample density throughout the differential absorption procedures due to the light interaction with nanocomposites. Thus, optical limiting identified for the low concentration CdS samples is much weaker than those of the higher concentration of Cd content. Cd/PMMA nanocomposite film of 3.33 wt% reduces the laser beams of both wavelengths operated at 632.8 nm and 533 nm. CdS/PMMA optical limiting arose from the current samples depending on its transmission ability of the incident light (see Fig. 4a, b). Both 1.66 and 3.33 wt% of CdS/PMMA films showed a block in the transmittance in the region from 190 to 630 nm (i.e., $T \approx 0$). CdS/PMMA has a good impact on the light blocking for the studied laser sources.

From the previous work (Yahia and Keshk 2017; Shkir et al. 2018; Assiri et al. 2019), the laser energy attenuation (i.e., optical limiting) depends primarily on the film
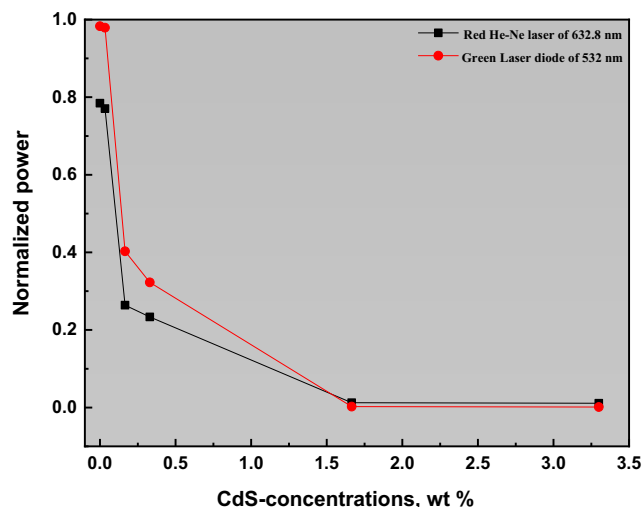
Fig. 10 The normalized power of CdS/PMMA nanocomposite films by using a red He-Ne laser of 632.8 nm, and a green laser diode of 532 nm

transmittance values for the operated laser beam of distinct wavelength (Elhosiny Ali et al. 2019). The attenuation and blocking of laser power increase as the transmittance approaches to zero. This proves the possibility of using flexible polymeric films as CUT-OFF laser filters (Yahia and Mohammed 2018). So, CdS/PMMA nanocomposite films have excellent optical limitation characteristics. Therefore, these nanocomposite films, especially with a higher content of CdS, can be used extensively in optoelectronic applications for CUT-OFF laser filters.

The photocatalytic performance of CdS/PMMA nanocomposites films

CdS/PMMA was used for the visible photocatalytic performance of RhB dye. The kinetics model of RhB photodegradation over CdS/PMMA catalysts obeys first-order Langmuir–Hinshelwood equation:

$$\ln(C/C_o) = K_1 t \qquad (7)$$

where C and C_o are dye concentrations at different time t and 0 times of visible light exposure, respectively, and K_1 is the reaction rate constant. The plotting of $\ln(C/C_o)$ versus time t (min) gives straight of slope K_1 (min^{-1}) value. In Fig. 11, the photodegradation rate was affected by the CdS content as follows: for pure PMMA (0.00834 min^{-1}), CdS/PMMA-0.033 wt% (0.02093 min^{-1}), CdS/PMMA-0.16 wt% (0.03427 min^{-1}) and CdS/PMMA-0.33 wt% (0.05069 min^{-1}), CdS/PMMA-1.66 wt% (0.06105 min^{-1}), and CdS/PMMA-3.3 wt% (0.07565 min^{-1}), respectively. The photocatalytic performance of the as-prepared material, as per the results, is influenced by the CdS/PMMA wt%. The rate constants of RhB are about pure PMMA < CdS/PMMA-0.033 wt% < CdS/PMMA-0.16 wt % < CdS/PMMA-

0.33 wt% < CdS/PMMA-1.66 wt % > CdS/PMMA-3.3 wt%.

Figure 12 showed the cycling experiments (i.e., stability) of CdS/PMMA nanocomposite films. Throughout five-time cycling tests, there is no noticeable reduction in the degradation of the studied films. CdS/PMMA showed excellent recycling performance. The generated photocurrent of pure PMMA was too weak to be detected under these conditions; however, PMMA acts as carrier transport. The generated 3.3 wt% CdS/PMMA photocurrent is much higher by 10 times than pure PMMA, indicating that the heterostructure efficiency was formed between CdS and PMMA interfaces to prevent the recombination of hole-electron pairs (Fan et al. 2016). Initially, the illumination of light-producing holes on the surface of the sample results in the photocurrent generation on the semiconductor surface. The gradual decrease of the photocurrent intensity occurred with time due to the recombination of the holes with the electrons (Yang et al. 2018). Therefore, 3.3 wt% of CdS/PMMA is more effective than pure PMMA because the electrons-holes generated by photons become easier to be separated.

The outstanding of the 3.3 wt% CdS/PMMA catalytic activity has been displayed among the full dye degradation that happened within 30 min of simulated sunlight. The photocatalytic output is compatible with the optical studies. The reaction rate is enhanced by incorporating a 3.3 wt% CdS/PMMA. The rate K_1 of 7.56×10^{-2} min^{-1} is 2.7 times higher than the rate constant produced by Jithesh Kavil et al. (2018), which was 2.8×10^{-2} min^{-1} that consequently 3.5 times TiO$_2$. They found that 10 wt% CdS/TiO$_2$ by Liu et al. (2019) was projected to have the largest K_1 value for RhB photodegradation due to the formation of better heterostructure between CdS nanoparticles and PMMA matrix. The computed K_1 values were 0.00317/min for pure PMMA, while it is equal 0.00714/min, 0.02467/min, 0.00288/min, and 0.00215/min for 5 wt%, 10 wt%, 20 wt%, and 30 wt%, respectively. Liu et al. (2019) reported that 10 wt% Cu$_2$–xSe/CdS was 7.8 times higher than the pure CdS. Benjamin et al. (2015) indicated that TiO$_2$-PMMA films have a better methyl orange photodegradation efficiency than the pure TiO$_2$, which provides a general advanced photocatalytic application. K_1 of TiO$_2$-PMMA films is about 0.0185 min^{-1}, which is 4.13 times less than 3.3 wt% CdS/PMMA films.

RhB photocatalytic mechanism using CdS/PMMA films

A suggested mechanism for RhB photodegradation was proposed under visible illumination in the presence of CdS/PMMA nanocomposite membranes based on the above findings and discussions. RhB photodegradation herein was affected by CdS nanoparticles and PMMA as a matrix. It can be observed in Scheme 1 that there is a limited energy gap of about 2.4 eV expelled from the valence band to the conduction
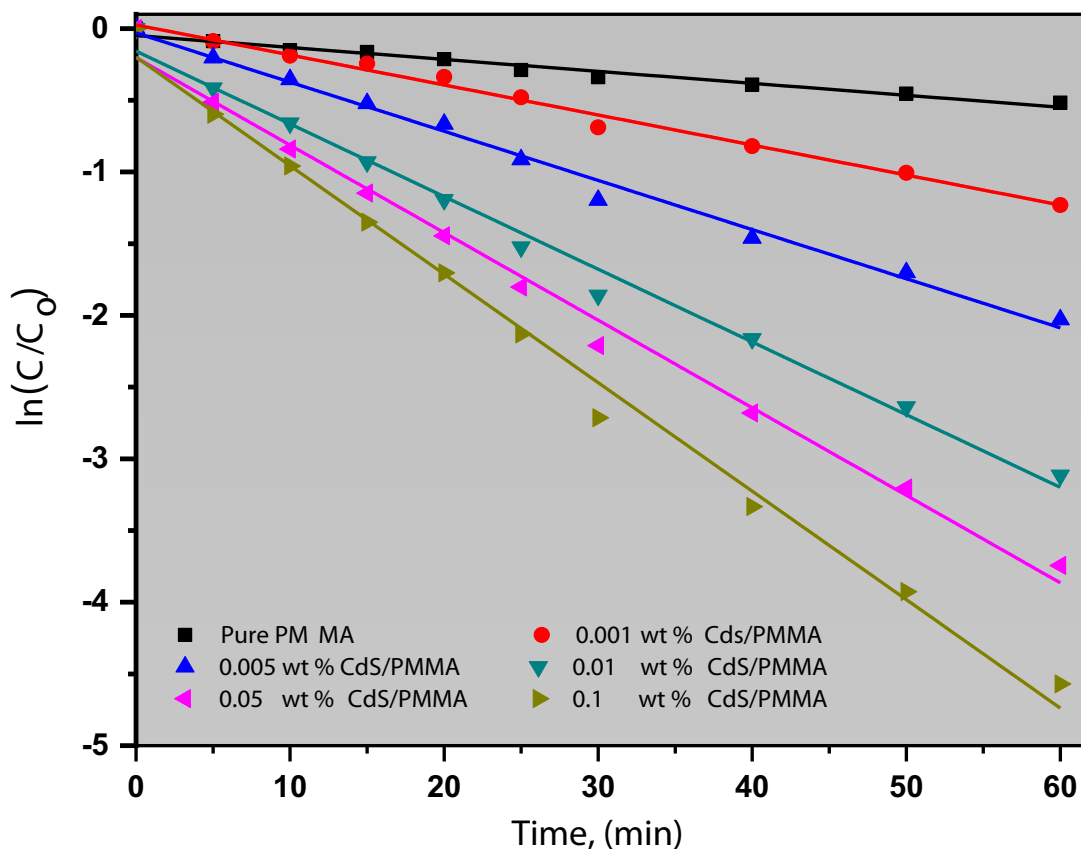
Fig. 11 Natural log of the ratio of RhB concentration (C) to the initial RhB concentration (C_o) a function of time for six representative samples with various CdS contents. The equations showed the least-squares fit to the first order

band of CdS utilizing visible radiation photons. The photogenerated electrons have been transmitted from conduction to the valence band after absorbing sufficient photons (Xue et al. 2014). Delocalization charge significantly decreases the electron-hole recombination rate and thus promotes the oxidation-reduction process. The O_2 traps CB electrons for $O_2 \cdot^-$ and H_2O_2 creation. These intermediates respond to form the $OH \cdot$, a strong oxidizing agent that can degrade

organic pollutants (Kalithasan et al. 2017). Prospective reactions to photocatalytic degradation of RhB are as follows:
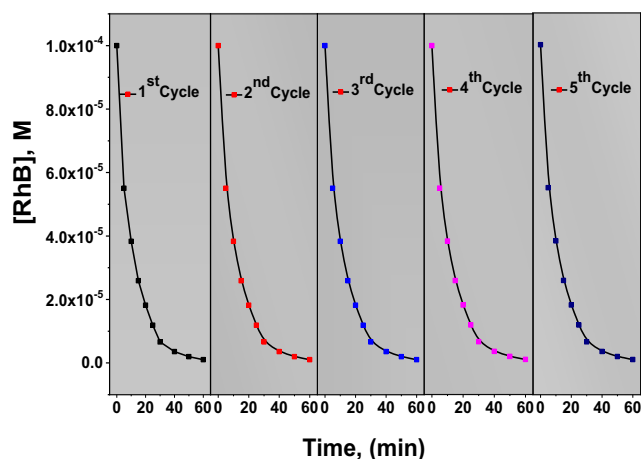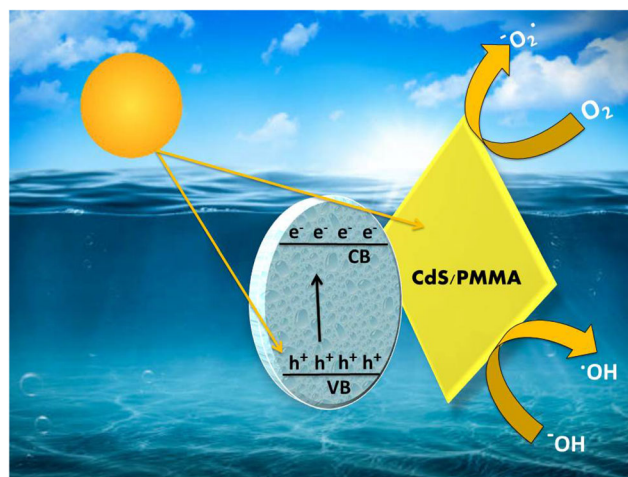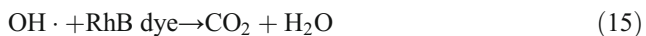
$$CdS + h\upsilon \rightarrow e^-_{CB} + h^+_{VB} \tag{8}$$

$$e^-_{CB} + O_2 \rightarrow O_2 \cdot^- \tag{9}$$
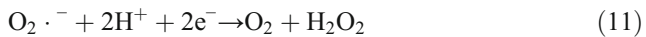
$$h^+_{VB} + OH^- \rightarrow OH \tag{10}$$

Fig. 12 Photodegradation of RhB by CdS/PMMA during five consecutive cycles ([RhB] = 10 mg/L)

Scheme 1 Schematic diagram of electron-hole pair separation and the proposed photocatalytic mechanism over CdS/PMMA polymeric nanocomposite films under visible light.

$$O_2 \cdot^- + 2H^+ + 2e^- \rightarrow O_2 + H_2O_2 \qquad (11)$$

$$O_2 \cdot^- + H_2O \rightarrow H_2O \cdot + OH^- \qquad (12)$$

$$H_2O \cdot + H_2O \rightarrow H_2O_2 + OH \qquad (13)$$

$$H_2O_2 \rightarrow 2OH \qquad (14)$$

$$OH \cdot + RhB\ dye \rightarrow CO_2 + H_2O \qquad (15)$$

The PMMA, as excellent carrier transport, played a role in reducing photogenerated e^-/h^+ pair recombination rates and prolong the photogenerated center life (Ying Mei et al. 2012). It helps raise the photostability of CdS nanoparticles against environmental conditions. PMMA was used as a matrix membrane due to its optical transparency. It is also facilitating the separation during the cyclic process (Yousif et al. 2014). It provides a higher nanoparticle semiconductor surface area. Eventually, OH· radicals and $O_2 \cdot^-$ % active species mineralize dye molecules into CO_2 and water.

The obtained CdS/PMMA nanocomposite films had long durability, stability, and reusability as elucidate through the characterization and applications. Moreover, it can be considered highly stable photocatalytic material, which is highly appreciated in the environmental applications. CdS have been reported to have a high ability to absorb visible light due to a narrow bandgap, thus contributing to enhancing its photodegradation efficiency (Zhong et al. 2019). Recently, the eco-friendly and low cost-effective technologies based on the polymeric nanocomposites were considered the primary objective and point of interest for most researchers (Zhong et al. 2020). Moreover, heterojunction photocatalysts can accelerate the photo-excited electron-hole separation in the photocatalytic application (Xu et al. 2020). It was noted that enhancing photocatalytic performance of materials based CdS was attributed to the charge separation, which can effectively reduce the recombination of electron-hole pairs (Liu et al. 2019).

Conclusion

Using the solution casting technique, efficient preparation was processed for a sequence of CdS/PMMA nanocomposite membranes. The structure of CdS/PMMA revealed the amorphous domains of the PMMA polymer, which increased with the increase of CdS concentrations. SEM images demonstrate that the CdS content in the PMMA matrix was uniformly dispersed, while the CdS nanoparticles agglomerated at the higher CdS content. The optical constants were analyzed via UV-Vis-NIR spectroscopy. It was discovered that the optical energy gap decreased. At the same time, the AC electrical conductivity and dielectric properties were enhanced by CdS doping owing to the enhanced density of localized states and leading to the lower energy bandgap. Increasing the CdS content leads to an increase in the extinction coefficient. The AC

electrical conductivity indicates a low-frequency plateau and high-frequency dispersion. By raising the CdS content in the PMMA matrix, the optical limiting is massively improved. From this consequence, it is concluded that CdS/PMMA nanocomposite films are regarded as promising candidates in the optical limiting and visible laser CUT-OFF filter techniques, i.e., laser power attenuation using CdS/PMMA nanocomposite membranes. CdS/PMMA has efficiently degraded RhB in aqueous solution in a short periodic time under visible illumination. Besides, CdS/PMMA retains its photocatalytic activity in RhB degradation during the recycling process. CdS/PMMA membrane exhibited a prospective recyclable photocatalytic performance for pollutant degradation. The work offers a new strategy for sophisticated photocatalyst polymeric membranes based on inorganic semiconductors CdS nanostructured in the PMMA matrix.

References

Ai Z, Zhao G, Zhong Y, Shao Y, Huang B, Wu Y, Hao X (2018) Phase junction CdS: high efficient and stable photocatalyst for hydrogen generation. Appl Catal B Environ 221:179–186

Ajibade PA, Mbese JZ (2014) Synthesis and characterization of metal sulfides nanoparticles/poly(methyl methacrylate) nanocomposites. Int J Polym Sci 2014:752394 8 pages

Al-Hosiny NM, Abdallah S, Moussa MAA, Badavi A (2013) Optical, thermophysical and electrical characterization of PMMA (CdSe QDs) composite films. J Polym Res 20:76

Al-Hussam AMA, Jassim SA (2012) Synthesis, structure, and optical properties of CdS thin films nanoparticles prepared by chemical bath technique. J Assoc Arab Univ Basic Appl Sci 11:27–31

Al-Taay HF, Shanan ZJ, Khaddum E, Abdalameer NK, Talal S, Nader R (2016) Optical and structural properties of CdS/PVA nanocomposites. J Appl Phys 8:73–79

Assiri MA, Manthrammel MA, Aboraia AM, Yahia IS, Zahran HY, Ganesh V, Shkir M, Al Faify S, Soldatov AV (2019) Kramers–Kronig calculations for linear and nonlinear optics of nanostructured methyl violet (CI-42535): new trend in laser power attenuation using dyes. Phys B Condens Matter 552:62–70

Benjamin DS, Lee GA, Bria SP, Daly CA Jr, Boyd JE (2015) Porous PMMA-titania composites: a step towards more sustainable photocatalysis. J Water Process Eng 8:179–185

Chan KS, Ami KAM, Hong LL, Hassan MF, Ismail M (2017) Investigation of morphological, structural and electrical properties of Cds/ PMMA nanocomposite film prepared by solution casting method. Int J Electrochem Sci 12:10023–10031

Choudhary S (2017) Structural and dielectric properties of (PEO–PMMA)–SnO 2 nanocomposites. Compos Commun 5:54–63

Choudhary S, Sengwa RJ (2016) Anomalous behaviour of the dielectric and electrical properties of polymeric nanodielectric poly(vinyl alcohol)–titanium dioxide films. J Appl Polym Sci 133:44568

Dang ZM, Zhang YH, Tjong SC (2004) Dependence of dielectric behavior on the physical property of fillers in the polymer-matrix composites. J Synth Met 146:79–84

Dixit M, Gupta S, Mathur V, Rathore KS, Sharma K, Saxena NS (2009) Study of glass transition temperature of PMMA and CdS-PMMA composite. Chalcogenide Lett 6(3):31–136

Elhosiny Ali H, Khairy Y, Algarni H, Elsaeedy HI, Alshehri AM, Alkharis H, Yahia IS (2019) The visible laser absorption property of chromium-doped polyvinyl alcohol films: synthesis, optical and dielectric properties. Opt Quant Electron 51:47

Fan XQ, Zhang LX, Li ML, Wang M, Zhou XX, Cheng RL, Zhou YJ, Shi JL (2016) α-Ferrous oxalate dihydrate: a simple coordination polymer featuring photocatalytic and photo-initiated Fenton oxidations. Sci China Mater 59:574

Hafizah NN, Mamat MH, Said CMS, Abidin MH, Rusop M (2013) Thermal degradation of nanocomposited PMMA/TiO2 nanocomposites. Mater Sci Eng 46:012045

Heiba ZK, Mohamed MB, Imam NG (2017) Optical and structural characteristics of CdSe/PMMA nanocomposites. J Polym Process Soc 2: 33

Ismail MM, Afify HH, El Shaarawy M, Shash NMH, Ashiry A, Battisha IK (2012) Aust J Basic Appl Sci 6(13):530–535

Jeon IY, Baek JB (2010) Nanocomposites derived from polymers and inorganic nanoparticles. J Mater 3:3654–3674

Jie J, Zhou ZJ, Zhou WH, Wun SX (2013) CdS and PbS quantum dots co-sensitized TiO2 nanorod arrays with improved performance for solar cells application. Mater Sci Semicond Process 16:435–440

Kalithasan N, Bajaj HC, Tayade RJ (2017) Direct sunlight driven photocatalytic activity of GeO2/monoclinic-BiVO4 nanoplate composites. Sol Energy 148:87–97

Kashiwagi T, Fagan J, Douglas JF (2007) Relationship between dispersion metric and properties of PMMA/SWNT nanocomposites. Polymer 48:4855–4866

Kavil J, Alshahrie A, Periyat P (2018) CdS sensitized TiO2 nano heterostructures as sunlight driven photocatalyst. Nano-Struct Nano-Objects 16:24–30

Kondawar SB, Acharya SA, Dhakate SR (2011) Microwave assisted hydrothermally synthesized nanostructure zinc oxide reinforced polyaniline nanocomposites. Adv Mater Lett 2(5):362–367

Liu Y, Shen S, Zhang J, Zhong W, Huang X (2019) Cu2−xSe/CdS composite photocatalyst with enhanced visible light photocatalysis activity. Appl Surf Sci 478:762–769

Mai SAH, Yahia IS (2019) Fabrication progress of selective and durable Ni2+-doped Ag3PO4 for visible-light degradation of various textile dyes. J Photochem Photobiol A 368:210–218

Maji P, Pande PP, Choudhary RB (2015) Effect of Zn(NO3)2 filler on the dielectric permittivity and electrical modulus of PMMA. Bull Mater Sci 38(2):417–424

Mansour Sh A, Elsad RA, Izzularab MA (2016) Dielectric properties enhancement of PVC nanodielectrics based on synthesized ZnO nanoparticles. J Polym Res 23:85 (8 pp)

Mervat IM, Fouad SS, Mehta N (2018) Correction to: Dielectric relaxation and thermally activated a.c. conduction in (PVDF)/(rGO) nanocomposites: role of rGO over different fillers. J Mater Sci Mater Electron 29:18271–18281

Miao F, Yu C, Lingling G, He N, Bai J, Lin Y, Zhan H (2009) CdS nanoparticles chemically modified PAN functional materials: preparation and nonlinear optical properties. Eur Polym J 45(4):1058–1064

Mohamed NBH, Haouari M, Zaaboub Z, Nafoutti M, Hassen F, Maaref H, Ouada HB (2014) Time resolved and temperature dependence of the radiative properties of thiol-capped CdS nanoparticles films. J Nanopart Res 16(1–17):2242

Mohammed MI (2018) Optical properties of ZnO nanoparticles dispersed in PMMA/PVDF blend. J Mol Struct 1169:9–17

Mohammed MI, Yahia IS (2018) Synthesis and optical properties of basic fuchsin dye-doped PMMA polymeric films for laser applications: wide scale absorption band. Opt Quant Electron 50:159

Motaung TE, Luyt AS, Bondioli F, Messori M, Saladino ML, Spinella A, Nasillo G, Caponetti E (2012) PMMA–titania nanocomposites: properties and thermal degradation behavior. Polym Degrad Stab 97:1325–1333

Mthethwa TP, Moloto MJ, De Vries A, Matabola KP (2011) Properties of electrospun CdS and CdSe filled poly (methyl methacrylate) (PMMA) nanofibers. J Mater Res Bull 46:569–575

Murcia López S, Bacariza MC, Villa K (2017) Controlled photocatalytic oxidation of methane to methanol through surface modification of beta zeolites. ACS Catal 7(4):2878–2885

Ning X, Zhen W, Wu Y, Lu G (2018) Inhibition of CdS photocorrosion by Al2O3 shell for highly stable photocatalytic overall water splitting under visible light irradiation. Appl Catal B Environ 226:373–383

Padmaja S, Jayakumar S, Balaji R, Sudakar C, Kumaravel M, Rajendran V, Rajkumar M, Radhamani AV (2013) Structural and optical properties of CdS/PEO nanocomposite solid films. Mater Sci Semicond Process 16:1502–1507

Padmaja S, Jayakumar S, Balaji R (2015) CdS:PMMA nanocomposite solid films with enhanced properties. Mater Technol 30(5):276–281

Parthibavarman M, Vallalperuman K, Sathishkumar S, Durairaj M, Thavamani K (2014) A novel microwave synthesis of nanocrystalline SnO2 and its structural optical and dielectric properties. J Mater Sci Mater Electron 25:730–735

Pichat P (2013) Photocatalysis and water purification: from fundamentals to recent applications. Wiley, Germany First Edition

Ranjbar M, Yousefi M, Nozari R, Sheshmani S (2013) Synthesis and characterization of cadmium thioacetamide nanocomposites using a facile sonochemical approach: a precursor for producing CdS nanoparticles via thermal decomposition. Int J Nanosci Nanotechnol 9:203–212

Shkir M, Khan MT, Ganesh V, Yahia IS, Haq B, Almohammedi A, Patil PS, Maidur SR, Al Faify S (2018) Influence of dye doping on key linear, nonlinear and optical limiting characteristics of SnO2 films for optoelectronic and laser applications. Opt Laser Technol 108: 609–618

Sugumaran S, Bellan CS, Muthu D, Raja S, Bheeman D, Rajamani R (2015) New transparent PVA-InTiO hybrid thin films: influence of InTiO on the structure, morphology, optical, and dielectric properties. Polym Adv Technol 26:1486–1493

Tauc J, Menth A, Wood D (1970) Optical and magnetic investigation of the localized states in semiconducting glasses. Phys Rev Lett 25: 749–752

Tripathi SK, Kaur R, Jyoti (2015) Investigation of non-linear optical properties of CdS/PS polymer nanocomposite synthesized by chemical route. Opt Commun 352:55–62

Tsai CY, Liu CW, Fan C (2017) Synthesis of a SnO2/TNT heterojunction nanocomposite as a high-performance photocatalyst. J Phys Chem C 121(11):6050–6059

Ummartyotin S, Bunnak N, Juntaro J, Sain M, Manuspiya H (2012) Hybrid organic-inorganic of ZnS embedded PVP nanocomposite flm for photoluminescent application. C R Phys 13(9–10):994–1000

Venkatram N, Narayana Rao D, Akundi MA (2005) Nonlinear absorption, scattering and optical limiting studies of CdS nanoparticles. J Optics Express 13:867–872

Vishal M, Sharma K (2013) Influence of CdS nano additives on the thermal conductivity of poly(vinyl chloride)/CdS nanocomposites. Adv Nanoparticle 2:205

Vishal M, Kuldeep SR, Kananbala S (2013) Evaluation of energy band gap, thermal conductivity, phase transition temperature and elastic response of PS/CdS semiconducting optical nanocomposite. World J Nano Sci Eng 3:93–99

Wang DS, Wang YH, Li XY, Luo QZ, An J, Yue JX (2008) Sunlight photocatalytic activity of polypyrroleeTiO2 nanocomposites prepared by 'in situ' method. Catal Commun 9:1162–1166

Wang M, Cai L, Wang Y, Zhou F, Xu K, Tao X, Chai Y (2017) Graphene-draped semiconductors for enhanced photocorrosion resistance and photocatalytic properties. J Am Chem Soc 139:4144–4151

Xu AJ, Wenguang T, Shen S, Lin Z, Gao N, Zhong W (2020) BiVO4@MoS2 core-shell heterojunction with improved photocatalytic activity for discoloration of Rhodamine B. Appl Surf Sci 528: 146949

Xue C, Wang T, Yang G, Yang B, Ding S (2014) A facile strategy for the synthesis of hierarchical TiO2/CdS hollow sphere heterostructures with excellent visible light activity. J Mater Chem A 2:7674–7679

Yahia IS, Keshk S (2017) Preparation and characterization of PVA/ Congo red polymeric composite flms for a wide scale laser filters. Opt Laser Technol 90:197–200

Yahia IS, Mohammed MI (2018) Facile synthesis of graphene oxide/ PVA nanocomposites for laser optical limiting: band gap analysis and dielectric constants. J Mater Sci Mater Electron 29:8555–8563

Yang H, Jin ZL, Wang GR, Liu DD, Fan K (2018) Light-assisted synthesis MoSx as a noble metal free cocatalyst formed heterojunction CdS/Co3O4 photocatalyst for visible light harvesting and spatial charge separation. Dalton Trans 47:6973–6985

Ying Mei XIE, Lu LV, Ming Hui LI, Cai PB, Qun C, Ming ZW, Xing ZQ (2012) Development of cation exchanger-based nano-CdS hybrid catalyst for visible-light photodegradation of rhodamine B from water. Sci China Chem 55(3):409–415

Yousif E, Salimon J, Salih N (2014) Mechanism of photostabilization of poly(methymethacrylate) films by 2-thioaceticacid benzothiazol complexes. Arab J Chem 7:306–311

Zhang L, Li F, Chen Y, Wang X (2011) Synthesis of transparent ZnO/ PMMA nanocomposite films through free-radical copolymerization of asymmetric zinc methacrylate acetate and in-situ thermal decomposition. J Lumin 131(8):1701–1706

Zhao R, Chen C, Li Q, Luo W (2008) Effects of stress and physical ageing on nonlinear creep behavior of poly (methyl methacrylate). J Cent S Univ Technol 15(1):582–588

Zhong W, Shen S, He M, Wang D, Wang Z, Lin Z, Wenguang T, Yu J (2019) The pulsed laser-induced Schottky junction via in-situ forming Cd clusters on CdS surfaces toward efficient visible light-driven photocatalytic hydrogen evolution. Appl Catal B Environ 258:117967

Zhong W, Wenguang T, Wang Z, Lin Z, Xu A, Ye X, Chen D, Xiao B (2020) Ultralow-temperature assisted synthesis of single platinum atoms anchored on carbon nanotubes for efficiently electrocatalytic acidic hydrogen evolution. J Energy Chem 51:280–228